Journal of Coordination Chemistry

ISSN: 0095-8972 (Print) 1029-0389 (Online) Journal homepage: http://www.tandfonline.com/loi/gcoo20

Synthesis, characterization, conduction, and dielectric properties of tetra tert-butylsulfanyl substituted phthalocyanines

Saida Kaipova, Hatice Dinçer & Ahmet Altindal

To cite this article: Saida Kaipova, Hatice Dinçer & Ahmet Altindal (2015) Synthesis, characterization, conduction, and dielectric properties of tetra tert-butylsulfanyl substituted phthalocyanines, Journal of Coordination Chemistry, 68:4, 717-731, DOI: 10.1080/00958972.2014.992340

To link to this article: http://dx.doi.org/10.1080/00958972.2014.992340

Accepted author version posted online: 27 Nov 2014.
Published online: 24 Dec 2014.

Journal of Coordination Chemistry, 2015
Vol. 68, No. 4, 717–731, http://dx.doi.org/10.1080/00958972.2014.992340

Synthesis, characterization, conduction, and dielectric properties of tetra *tert*-butylsulfanyl substituted phthalocyanines

SAIDA KAIPOVA†, HATICE DINÇER*† and AHMET ALTINDAL‡

†Department of Chemistry, İstanbul Technical University, İstanbul, Turkey
‡Department of Physics, Yıldız Technical University, İstanbul, Turkey

(*Received 12 August 2014; accepted 30 October 2014*)

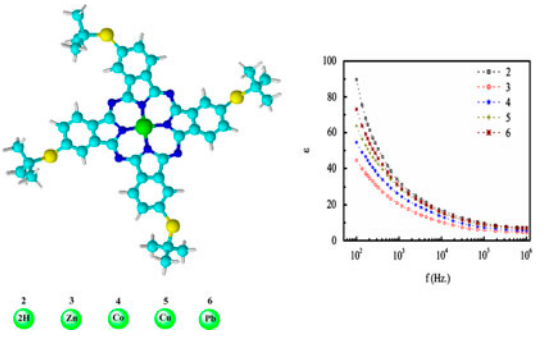

The *tert*-butylsulfanylphthalonitrile has been prepared with optimized synthetic procedure. Metal free (H_2Pc) and metallo phthalocyanines (Pcs) (ZnPc, CoPc, CuPc, PbPc) have been synthesized by cyclotetramerization of *tert*-butylsulfanylphthalonitrile in the presence of DBU and metal salts. Thus, *tert*-butylsulfanyl groups enhance the solubility, shift the Q band absorption to the red visible region, and inhibit efficient cofacial interaction of the Pcs (**2–6**) as evaluated by UV–vis spectra. The electrical conduction and dielectric properties of the synthesized Pc thin films sandwiched between indium tin oxide and aluminum electrodes (ITO–Pc–Al) were investigated from 300 to 500 K. At low bias voltage the conduction is ohmic while at high bias voltage the conduction becomes space charge limited with an exponential distribution of traps. The measured ac conductivity data are discussed in terms of classical models based on pair approximation. It was found that the ac conductivity obeys the power law given by $\sigma_{ac} = \sigma_0\omega^s$, in which the frequency exponent s decreases with temperature. The real and imaginary parts of the impedance are found to be dependent on both frequency and temperature.

Keywords: *Tert*-butylsulfanyl; Phthalonitrile; Phthalocyanine; Conduction; Dielectric properties

1. Introduction

The past two decades have seen a dramatic increase in diversity of research of phthalocyanines (Pcs) such as chemical sensors, electrochromism, liquid crystals, Langmuir–Blodgett

*Corresponding author. Email: dincerhat@itu.edu.tr

films, semiconductors, functional polymers, photodynamic cancer therapy, nonlinear optical applications, catalysis, and solar energy conversion [1–11]. The majority of these applications take advantage of the unique optical (specifically low-energy Q band) and redox properties of phthalocyanines which can be fine-tuned using appropriate peripheral substituents [12]. Many studies have been performed to develop new Pc derivatives with distinct and well-defined physical, chemical, and electronic properties that display characteristics useful for particular applications [13].

The basic approach for peripheral substitution is the tetramerization of the substituted phthalocyanine precursors and leads to a controlled number of substituents in the target phthalocyanine. Useful precursors for this method include substituted derivatives of phthalonitriles. *Tert*-butyl substituents on phthalocyanines are common and *tert*-butylphthalonitrile is commercially available [14–17]. The synthesis of alkylthio-substituted phthalonitriles is also easy, and especially the substitution of dichlorophthalonitrile with alkylthiols is well known [18–21]. The aggregation behavior of pcs limits their use in several applications. Substitution with bulky substituents such as *tert*-butyl suppresses the aggregation of pcs and enhances their solubilities. In addition, alkylthio groups furnish the red shift in the electronic absorption spectrum which is a desirable property for several applications. Tetra-substituted manganese phthalocyanine bearing *tert*-butylsulfanyl groups on peripheral positions have been reported by Dolotova *et al.* in 1992, prepared from *tert*-butylsulfanyl-substituted phthalonitrile compound [22]. Owing to potential applications in photodiodes, photovoltaic cells, and gas-sensitive devices, extensive research on phthalocyanine compounds and their derivatives has been carried out [23, 24]. The relaxation process and electrical conduction mechanisms in these classes of organic semiconductors play an important role and are often the deciding factors about the suitability of the material for particular device applications. Hence, a study of dc and ac conductivity in these materials indicates the nature of the localized states near the band edges below the conduction and above the valance bands produced by substitution disorders which control many of the opto-electronic properties.

Here, we describe the modified synthesis of *tert*-butylsulfanylphthalonitrile by reacting 2-methylpropane-2-thiol with 4-nitrophthalonitrile in mild conditions. The syntheses of highly soluble metal free and metallo (Zn, Co, Cu, Pb) phthalocyanine derivatives have also been achieved. Substitution at the peripheral positions of pcs with *tert*-butylsulfanyl moieties enhances the solubility and avoids aggregation in many solvents. Both dc and ac behavior of the spin-coated films of these phthalocyanine compounds were studied by using complex impedance spectroscopy. In addition, the dielectric behavior of the films has also been investigated as a function of temperature and frequency.

2. Experimental

2.1. *Materials and equipment*

All chemicals were of reagent grade quality obtained from commercial sources and used without purification. 4-Nitrophthalonitrile, 2-methyl-2-propanethiol and 1,8-diazabicyclo [5.4.0]undec-7-ene (DBU) were purchased from Aldrich. All solvents used for the syntheses were of analytical grade. Column chromatography was performed on silica gel 60 for purification (Merck Kieselgel 60 (0.040–0.063 mm)). The homogeneity of the products was tested in each step by thin layer chromatography (Merck aluminum sheets with silica gel 60 F254).

IR spectra were recorded on a Perkin Elmer Spectrum One FT-IR spectrometer with ATR capability; electronic spectra were recorded on a Scinco SD 1000 single-beam ultraviolet-visible (UV–vis) spectrophotometer using 1 cm path length cuvettes at room temperature. The ^{1}H NMR and ^{13}C NMR spectra were recorded on Agilent VNMRS (500 MHz for ^{1}H and 125 MHz for ^{13}C). Elemental analyses were performed on a Thermo Flash EA 1112. Mass spectra were performed on Bruker Microflex MALDI-TOF/MS and Perkin Elmer Clarus 500 mass spectrometers.

2.2. *Synthesis and characterization*

2.2.1. 4-(*Tert*-butyl)sulfanyl-phthalonitrile (1). 4-Nitrophthalonitrile (1 g, 5.75 mM) and 2-methyl-2-propanethiol (1.17 mL, 10.35 mM) were dissolved in 20 mL anhydrous dimethylformamide (DMF). After stirring for 10 min anhydrous K_2CO_3 (2.15 g, 15.5 mM) was added by stirring. The reaction mixture was held at 45 °C for 24 h under N_2. Then, the mixture was poured into ice water and the precipitate was filtered off, washed by water, and dried. The desired compound was obtained as a white powder without further purification. Yield: 1.08 g (87%), melting point (m.p.) 60–63 °C. FT-IR γ (cm^{-1}): 3071, 2923, 2867, 2852, 2231 (CN), 1553, 1489, 1462, 1371, 1258, 1153 (Ar–S–C), 1090, 959 (C–H). ^{1}H NMR ($CDCl_3$): δ, ppm 7.91 (Ar–H, s, 1H), 7.85 (Ar–H, d, 1H), 7.73 (Ar–H, d, 1H), 1.36 (CH_3, s, 9H). ^{13}C NMR ($CDCl_3$): δ, ppm 142.56, 141.78, 136.45 (Ar–CH), 138.99 (Ar–C–S), 115.19 (Ar–C–CN), 116.56 (CN), 41.76 (C–S), 31.04 (–CH_3). GC–MS: *m/z* ($C_{12}H_{12}N_2S$) found = 216.00 (Calcd for [M]$^{+}$ 216.30). Calculated for $C_{12}H_{12}N_2S$: C, 66.63; H, 5.59; N, 12.95; S, 14.82%. Found: C, 66.12; H, 5.65; N, 12.71; S, 14.24%.

2.2.2. 2(3),9(10),16(17),23(24)-Tetrakis(tert-butylsulfanyl)phthalocyanine (2). Compound **1** (0.1 g, 0.46 mM) and a catalytic amount of DBU in *n*-pentanol (1 mL) were heated at 140 °C for 24 h under N_2. The mixture was cooled to room temperature and poured into 30 mL methanol. Blue-green precipitate was filtered off and washed by methanol several times. The residue was purified by column chromatography on silica gel using DCM/methanol 100 : 2 as the eluent to afford metal-free phthalocyanine. Yield: 0.065 g (65%). FT-IR γ (cm^{-1}): 3290, 2981, 2862, 1604, 1501, 1363, 1336, 1303, 1253, 1160, 1105, 1008, 896, 829, 741. ^{1}H NMR ($CDCl_3$): δ, ppm 7.83 (Ar–H, br, 4H), 7.54 (Ar–H, br, 4H), 7.34 (Ar–H, br, 4H), 1.45 (–CH_3, m, 36H), –6.89 (N–H, s, 2H). ^{13}C NMR ($CDCl_3$): δ, ppm 146.14, 137.41, 135.74, 134.34, 129.76, 121.26 (Ar–C), 46.71 (C–S), 31.37, 30.30 (–CH_3). UV–vis (THF) λ_{max}/nm: 343,666,701; MALDI-TOF-MS *m/z* ($C_{48}H_{50}N_8S_4$) found = 867.623 (Calcd for [M]$^{+}$ 867.22), calculated for $C_{48}H_{50}N_8S_4$: C, 66.48; H, 5.81; N, 12.92; S, 14.79%. Found: C, 66.36; H, 5.76; N, 12.97; S, 14.84%.

2.2.3. General procedure for the synthesis of metallo phthalocyanines (3–6). A mixture of **1** (0.46 mM, 0.10 g), metal salts (0.154 mM, 0.028 g Zn $(OAc)_2$, 0.020 g $CoCl_2$, 0.027 g $Cu(OAc)_2$, and 0.055 g $Pb(OAc)_2{\cdot}3H_2O$) and a catalytic amount of DBU in *n*-pentanol (1 mL) was heated at 140 °C with stirring for 24 h under N_2. After cooling to room temperature, the reaction mixture was precipitated by adding methanol. The precipitate was filtered off and washed with methanol several times.

2.2.3.1. *2(3),9(10),16(17),23(24)-tetrakis(tert-butylsulfanyl)phthalocyaninatozinc(II) (3).* The dark blue precipitate was purified by column chromatography on silica gel using THF : hexane (100) as eluent. Yield: 0.063 g (59%). FT-IR γ (cm^{-1}): 2957, 2842, 1602, 1484, 1431, 1362, 1331, 1306, 1230, 1141, 1041, 909, 860, 802. ^{1}H NMR ($CDCl_3$): δ, ppm 7.84 (Ar–H, br, 4H), 7.74 (Ar–H, br, 4H), 7.45 (Ar–H, br, 4H), 1.25 (–CH_3, br, 36H). ^{13}C NMR ($CDCl_3$): δ, ppm 150.29, 146.31, 136.88, 135.34, 131.14, 128.67, 124.83, 121.40 (Ar–C), 46.59 (C–S), 31.13, 29.88 (–CH_3). UV–vis (THF) λ_{max}/nm: 354, 678; MALDI-TOF-MS *m/z* ($C_{48}H_{48}N_8S_4Zn$) found = 930.434 (Calcd for $[M]^+$ 930.60). Calculated for $C_{48}H_{48}N_8S_4Zn$: C, 61.95; H, 5.20; N, 12.04; S, 13.78%. Found: C, 62.03; H, 5.28; N, 12.11; S, 13.86%.

2.2.3.2. *2(3),9(10),16(17),23(24)-tetrakis(tert-butylsulfanyl)phthalocyaninatocobalt(II) (4).* The dark blue precipitate was purified by column chromatography on silica gel using DCM : methanol (100 : 10) as eluent. Yield: 0.072 g (68%). FT-IR γ (cm^{-1}): 2957, 2857, 1602, 1522, 1443, 1390, 1362, 1332, 1305, 1252, 1141, 1095, 1046, 931, 898, 828, 750. UV–vis (THF) λ_{max}/nm: 329, 667; MALDI-TOF-MS *m/z* ($C_{48}H_{48}N_8S_4Co$) found = 924.229 (Calcd for $[M]^+$ 924.14). Calculated for $C_{48}H_{48}N_8S_4Co$: C, 62.38; H, 5.24; N, 12.13; S, 13.88%. Found: C, 62.26; H, 5.17; N, 12.18; S, 13.95%.

2.2.3.3. *2(3),9(10),16(17),23(24)-tetrakis(tert-butylsulfanyl)phthalocyaninatocopper(II) (5).* The bluish crude product was purified by column chromatography on silica gel using DCM : methanol (100 : 5) as eluent. Yield: 0.069 g (65%). FT-IR γ (cm^{-1}): 2959, 2847, 1600, 1504, 1440, 1390, 1362, 1339, 1304, 1138, 1095, 919, 829, 744. UV–vis (THF) λ_{max}/nm: 349, 678; MALDI-TOF-MS *m/z* ($C_{48}H_{48}N_8S_4Cu$) found = 928.040 (Calcd for $[M]^+$ 928.75. Calculated for $C_{48}H_{48}N_8S_4Cu$: C, 62.07; H, 5.21; N, 12.06; S, 13.81%. Found: C, 61.98; H, 5.13; N, 12.14; S, 13.89%.

2.2.3.4. *2(3),9(10),16(17),23(24)-tetrakis(tert-butylsulfanyl)phthalocyaninatolead(II) (6).* The blue–green crude product was purified by flash column chromatography on silica gel using first methanol then DCM as eluent. Yield: 0.045 g (37%). FT-IR γ (cm^{-1}): 2961, 2852, 1601, 1391, 1363, 1340, 1291, 1259, 1072, 1038, 904, 796, 741. ^{1}H NMR ($CDCl_3$): δ, ppm 9.36–9.11 (Ar–H, br, 4H), 8.28 (Ar–H, br, 4H), 7.96–7.78 (Ar–H, br, 4H), 1.43 (–CH_3, m, 36H). ^{13}C NMR ($CDCl_3$): δ, ppm 151.49, 142.29, 136.87, 135.76, 131.10, 128.23, 125.49, 123.35 (Ar–C), 47.60 (C–S), 31.05, 30.30 (–CH_3). UV–vis (THF) λ_{max}/nm: 346,711; MALDI-TOF-MS *m/z* ($C_{48}H_{48}N_8S_4Pb$) found = 1072.630 (Calcd for $[M]^+$ 1072.41. Calculated for $C_{48}H_{48}N_8S_4Pb$: C, 53.76; H, 4.51; N, 10.45; S, 11.96%. Found: C, 53.67; H, 4.46; N, 9.37; S, 12.05%.

2.3. *Dc and ac measurements*

Metal-semiconductor-metal (MSM) capacitive devices were fabricated in a sandwich configuration with an active conduction area of 4.5×10^{-6} m^2. A photo resist spinner (Specialty Coatings Systems Inc., Model P 6700 Series) was employed to deposit Pc films onto a previously well cleaned ITO-coated glass substrate by spinning a small volume of the spreading solution at constant speed. The spreading solution was prepared by dissolving phthalocyanines in chloroform. Spinning was continued for 60 s in order to allow complete evaporation of the solvent, producing a uniform film. The resulting films were then heated

at 90 °C for 1 h to ensure removal of the residual solvent in the films. Elipsometric technique was used to measure the thickness of the polymer film. After deposition of the phthalocyanines films, substrate was immediately placed in a vacuum system for the top contact deposition processes. The circular top contacts on the Pc layer were formed by thermal evaporation of Al at pressure of approximately 1.0×10^{-5} mbar using an Edwards Auto 500 thermal evaporator system. Current (I) was measured from 300 to 420 K as a function of applied voltage (V) for ITO/Pc/Al structures using a Keithley 6517A electrometer. The frequency dependent conductivity and impedance spectroscopy measurements on Pc films were also carried out in the frequency range of 100 Hz–1×10^6 Hz between 300 and 500 K. Data of I–V and impedance measurements were recorded using a computer and a GPIB data transfer card. All measurements were performed under vacuum ($\leq 10^{-3}$ mbar) and in the dark.

3. Results and discussion

3.1. *Synthesis and characterization*

Dolotova *et al.* described the synthesis of *tert*-butylsulfanylphthalonitrile (**1**) by substitution of 4-nitrophthalonitrile with 2-methylpropane-2-thiol in the presence of triethylamine in DMF [22]. In our case, the reaction was performed between 4-nitrophthalonitrile and 2-methylpropane-2-thiol in DMF using potassium carbonate as the base at room temperature for 24 h in high yield (scheme 1). We obtained *tert*-butylsulfanylphthalonitrile (**1**) in milder conditions than its previously described synthesis. The structure of **1** was fully characterized by a combination of spectroscopic techniques such as FT-IR, ^{1}H NMR, ^{13}C NMR, GC–MS, and elemental analysis. The characteristic vibrations corresponding to CN, Ar–S–C, aromatic C–H, and aliphatic –CH_3 of *tert*-butyl groups at 2231, 1153, 3071, and 2923–2852 cm^{-1} were observed for **1** in the FT-IR spectrum. In the ^{1}H NMR spectrum of **1**, aromatic protons appeared as singlet at 7.91 and doublets at 7.85, 7.73, –CH_3 protons as singlet at 1.36 ppm. ^{13}C NMR spectrum of **1** shows typical chemical shifts for aliphatic carbons (31.04 ppm), C–S carbon (41.76 ppm), nitrile carbons (around 116 ppm), Ar–C–S carbon (138.99 ppm), and aromatic carbons (142.56–136.45 ppm). The mass spectrum and elemental analysis data of phthalonitrile (**1**) confirmed the proposed structure as indicated in the Experimental section.

In the case of phthalocyanines (**2–6**), the disappearance of the CN bands in the IR spectra highlights the cyclotetramerization of the phthalonitrile compound (**1**). IR spectra of the five complexes (**2–6**) are similar in most peaks with the exception of **2** showing an inner core –N–H stretch at 3290 cm^{-1}.

The ^{1}H NMR spectra of H_2Pc (**2**), ZnPc (**3**), and PbPc (**6**) have almost the same chemical shifts and somewhat broader than the corresponding signals in the phthalonitrile compound (**1**). The inner core –NH protons of the metal-free phthalocyanine (**2**) were observed at −6.89 ppm. H_2Pc (**2**), ZnPc (**3**), and PbPc (**6**) show the typical ^{13}C NMR shifts as indicated in the Experimental section. The disappearance of the peak associated with the nitrile carbon of **1** at ~116 ppm confirms the pc formation with the new peak around 150 ppm for **2**, **3**, and **6**. In the mass spectra of phthalocyanines (**2–6**), the molecular ion peaks were observed at *m/z* 867.623 $[M]^+$ for **2**, 930.434 $[M]^+$ for **3**, 924.229 $[M]^+$ for **4**, 928.040 $[M]^+$ for **5**, and 1072.630 $[M]^+$ for **6**. The mass spectra of **2** and **6** have been chosen to illustrate molecular ion peaks and fragment ions [figure 1(a) and (b)].

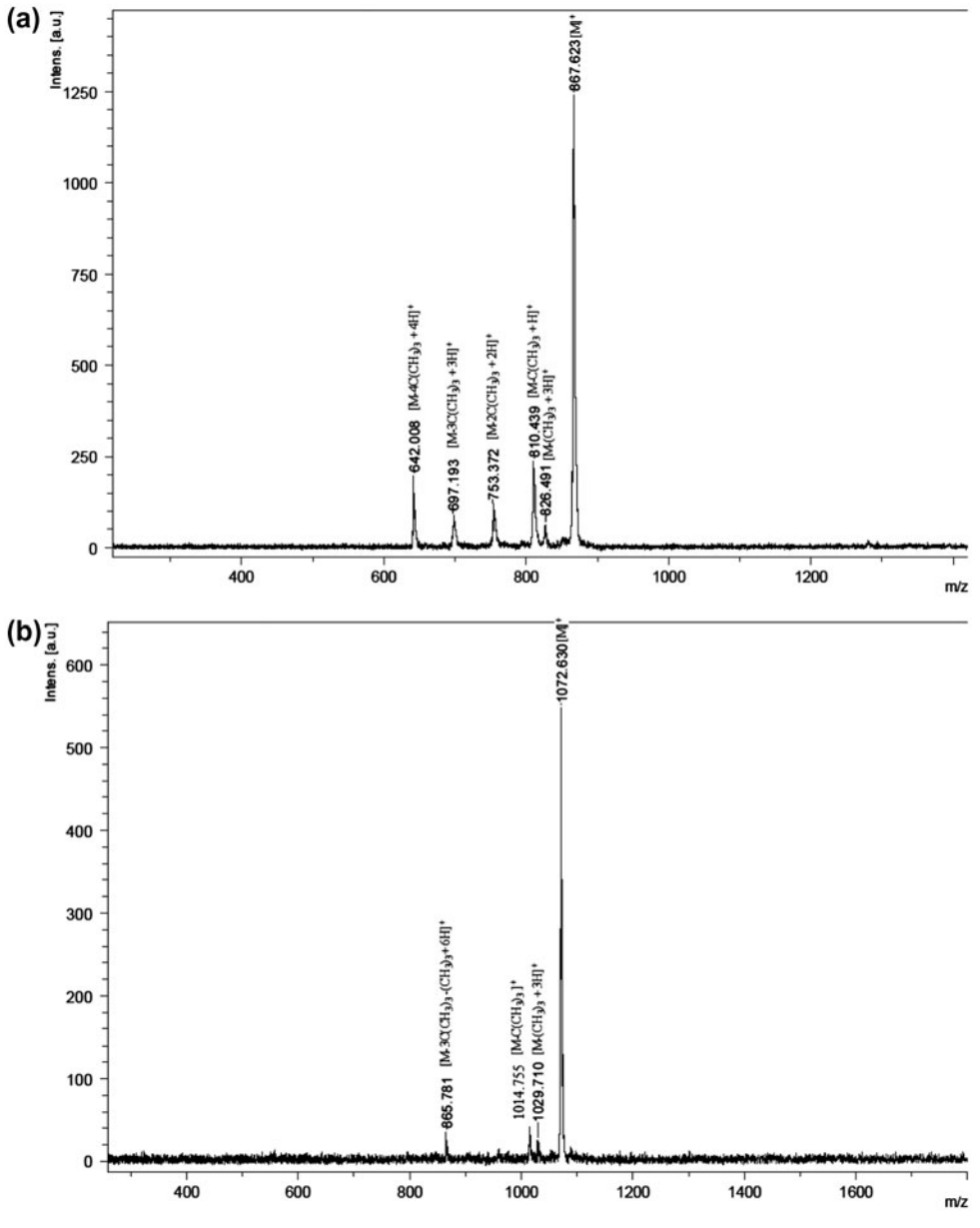

Figure 1. MALDI-TOF MS spectra of (a) H_2Pc (**2**) and (b) PbPc (**6**).

Satisfactory yields for all the target phthalocyanines (**2–6**) ranged from 37 to 68%. These complexes exhibit enhanced solubility in common organic solvents due to the tetra substitution of *tert*-butylsulfanyl groups.

In the electronic absorption spectra studies, the effects of metal and substituent on spectroscopic and aggregation properties of phthalocyanine derivatives (**2–6**) were investigated in different solvents (toluene, DCM, THF, and DMF). The λ_{max} absorption of the Q-bands

Table 1. Spectral data for phthalocyanines (**2–6**) in different solvents.

Pcs	λ_{max}/nm ($\log\varepsilon$/dm^3 mol^{-1} cm^{-1})			
	Toluene	DCM	THF	DMF
2	342(5.04), 669(5.25), 705(5.34)	343(5.12), 667(5.38), 702(5.4)	343(5.36), 666(5.48), 701 (5.54)	341(5.34), 667(5.23), 701(5.26)
3	363(4.76), 685(5.31)	351(4.82), 682(5.29)	354(4.76), 678(5.31)	357(4.63), 681(5.31)
4	331(5.08), 674(5.29)	326(5.11), 673(5.29)	329(5.16), 667(5.27)	332(5.14), 668(5.29)
5	345(4.82), 682(5.30)	342(4.83), 682(5.29)	349(4.84), 678(5.33)	349(4.88), 680(5.31)
6	349(4.82), 721(5.29)	347(4.83), 721(5.29)	346(4.85), 711(5.30)	347(4.72), 711(5.26)

of phthalocyanines (**2–6**) in toluene, DCM, THF, and DMF are listed in table 1. Unlike the spectra of metallo phthalocyanines (**3–6**), H_2Pc (**2**) shows a characteristic splitting of the Q-band around 667, 702 nm in different solvents. CoPc (**4**) displays Q band around 667–674 nm in different solvents whereas ZnPc (**3**) and CuPc (**5**) have nearly the same values around 678–685 nm and illustrate ~8–13 nm bathochromic shifts according to CoPc (**4**) analog. As shown in table 1, PbPc (**6**) has the largest bathochromic shift when compared to CoPc (**4**) around 43–48 nm, ZnPc (**3**) and CuPc (**5**) around 30–39 nm, respectively. Figure 2 shows that the largest shifts due to the metal effect are observed in DCM for phthalocyanines (**3–6**). To reveal the solvent effect, comparison of the λ_{max} of phthalocyanines (**2–6**) was studied in four solvents with different polarities (toluene < DCM < THF < DMF). The spectra of **3–5** show a small change of the maximum of the Q band from 685, 674, and 682 nm in toluene to 681, 668, and 680 nm in DMF. In the case of PbPc (**6**), relatively large negative solvatochromism from 721 nm in toluene to 711 nm in DMF was found (figure 3). The aggregation behavior of phthalocyanines usually can be evidenced by the broadening and blue shift of the Q-band with decrease in intensity. The electronic spectra of all phthalocyanines (**2–6**) showed single (narrow) Q bands in four different solvents in the

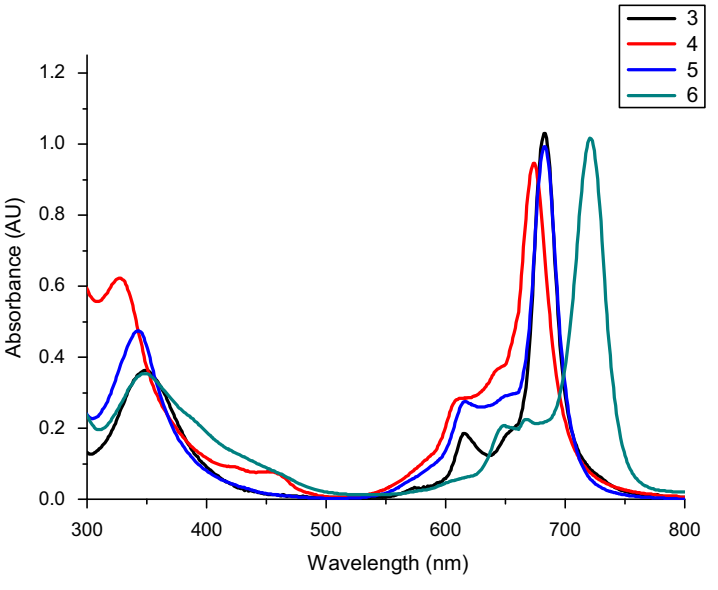

Figure 2. Electronic absorption spectra of metallo phthalocyanines (**3–6**) in DCM (~5 × 10^{-6} M dm^{-3}).

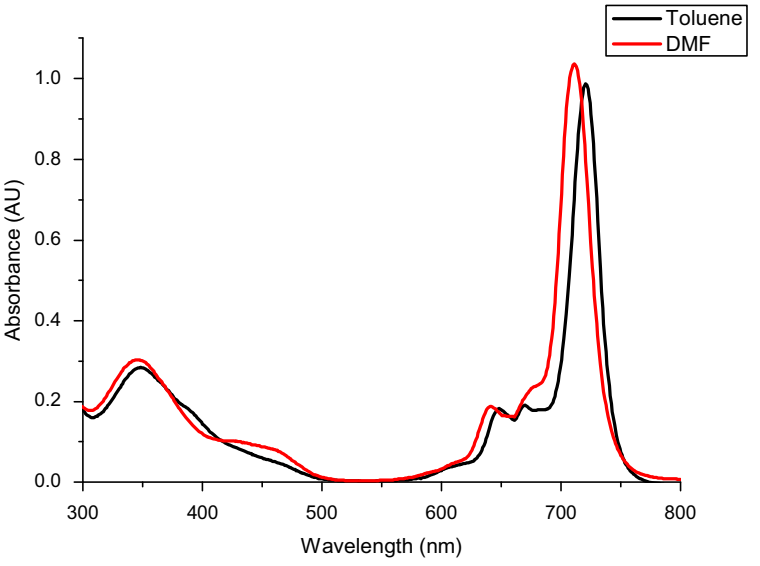

Figure 3. Electronic absorption spectra of **6** in toluene (black line) and DMF (red line) (~5×10^{-6} M dm^{-3}) (see http://dx.doi.org/10.1080/00958972.2014.992340 for color version).

concentrations ranging from 10×10^{-6} to 1×10^{-6} M (figure 4 as example for **3** (a) in THF and (b) in DMF), suggesting that the *tert*-butylsulfanyl groups prevent aggregation between Pc macrocycles.

3.2. *Dc behavior of ITO/Pc/Al devices*

In all the MSM devices investigated, the current density–voltage (J–V) curves showed an Ohm's law region at low fields followed by a power law region at high fields. Figure 5 shows the room temperature J–V characteristics of ITO/Pc/Al structures in the log–log scale. It can be clearly seen that the J–V characteristics are nonlinear and there is a well-defined voltage of V_t for transition from the ohmic to nonohmic behavior. This type of J–V characteristic has been extensively observed in Au/ZnPc/Au [25], Au/CoPc/Au [26], and recently also in Au/zinc phthalocyanine doped with tetrafluorotetracyanoquinodimethane/Au devices [27]. In all of these reports, a linear dependence of J on V with a slope of unity at lower voltages and a power law ($J \alpha V^m$) with $m > 2$ dependence at higher voltages have been observed.

There are different conduction mechanisms operating in the device depending on applied voltage (figure 5). At lower potential bias, the forward J–V relations are linear with slopes between $0.72 \leq m \leq 0.92$, indicating that the conduction mechanism may be described by Ohm's law [28]. In the ohmic region, the J–V dependence should be of the form,

$$J = q\mu p_0 \frac{V}{t} \tag{1}$$

where q is the electronic charge, μ is the mobility of charge carriers, V is the applied voltage across the device, t is the electrode separation, and p_0 is the thermally generated carrier concentration which is given by,

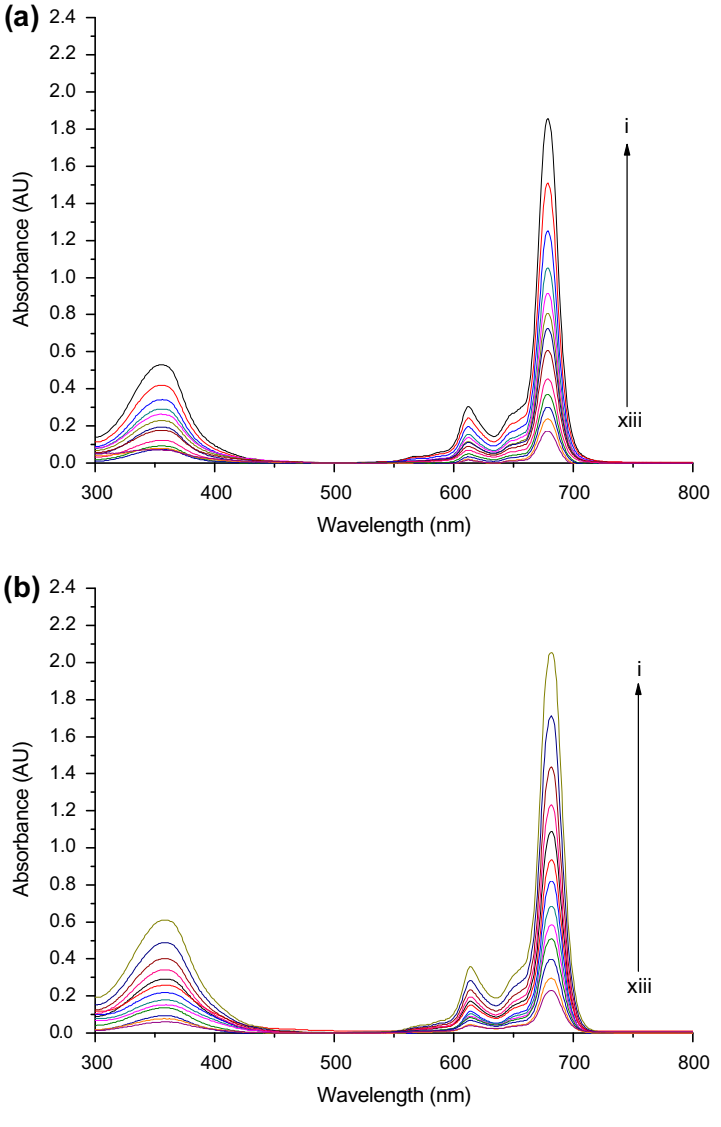

Figure 4. Electronic absorption spectra of **3** at various concentrations: (i) 10×10^{-6}, (ii) 8×10^{-6}, (iii) 6.6×10^{-6}, (iv) 5.7×10^{-6}, (v) 5×10^{-6}, (vi) 4.4×10^{-6}, (vii) 4×10^{-6}, (viii) 3.3×10^{-6}, (ix) 2.5×10^{-6}, (x) 2.1×10^{-6}, (xi) 1.7×10^{-6}, (xii) 1.4×10^{-6}, (xiii) 1×10^{-6} M dm^{-3} (a) in THF and (b) in DMF.

$$p_0 = N_v \exp - \left(\frac{E_F}{k_T}\right) \tag{2}$$

where E_F is the separation of the Fermi level from the valence band edge, k is the Boltzmann constant, T is the absolute temperature, and N_v is the density of states in the valence band. The value of E_F and the mobility μ can be obtained from plot of log (J) *versus* inverse temperature in the ohmic region of the measured J–V characteristics. Figure 6 is the

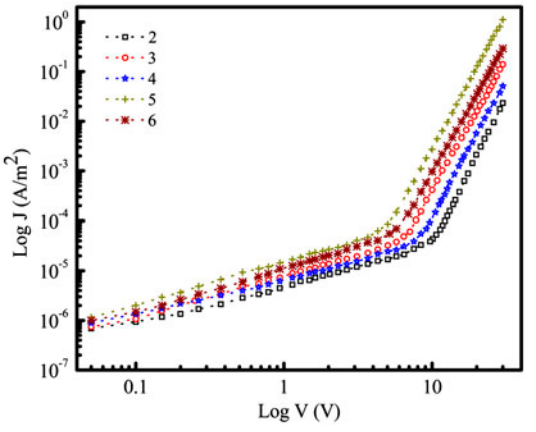

Figure 5. Room temperature *J–V* characteristics of the ITO/Pc/Al structures.

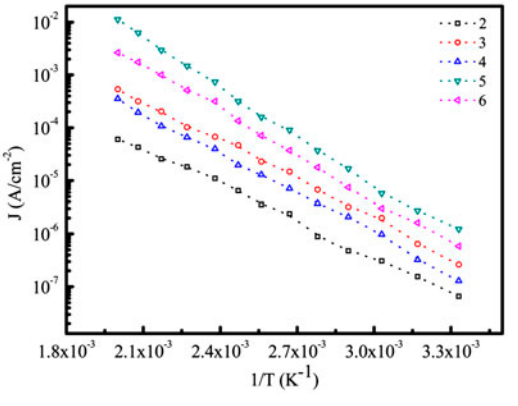

Figure 6. Log *J vs.* (1/*T*) plot for the films of **2–6** in the ohmic region.

plot of log (*J*) against (1/*T*) in the ohmic region for all films. As can be seen from figure 6 the graphs are almost straight lines where slopes of the lines yield the value of E_F and the intercept provides the value of the mobility of charge carriers, which were obtained and listed in table 2.

Table 2. Calculated electrical parameters for **2–6**.

Compound	E_F (eV)	μ ($m^2 sn^{-1} V^{-1}$)	P_0 (m^{-3})
2	0.43	3.82×10^{-9}	4.39×10^{19}
3	0.46	8.43×10^{-8}	9.22×10^{19}
4	0.45	7.88×10^{-8}	8.45×10^{19}
5	0.57	4.40×10^{-7}	4.56×10^{18}
6	0.53	3.10×10^{-7}	3.70×10^{18}

It is clear from figure 5 that, at higher applied bias voltages, current increases more rapidly and Ohm's law breaks down. In the higher voltage region, the slopes of log J–log V curves were 6.0, 5.3, 5.6, 5.4, and 5.2 for the films of **2–6**, respectively. As in our case, the slopes which are greater than 2 clearly suggest that the space charge limited current controlled by exponentially distributed trapping levels (SCLC) is the dominant mechanism [26, 29]. The J–V dependence in the SCLC region is given by,

$$I = q\mu A N_{\mathrm{v}} \left(\frac{\varepsilon}{qP_0kT_{\mathrm{t}}}\right)^{L} \left(\frac{V^{L+1}}{t^{2L+1}}\right) \tag{3}$$

where N_{V} is the effective density of states at the valence band edge, ε is the permittivity of polymer film, and k is the Boltzmann's constant. P_0 is the trap density per unit energy range at the valence band edge, the term $(L + 1)$ represents the power exponent factor, and L is the ratio T_{t}/T where T is the absolute temperature and T_{t} is a temperature parameter, which characterizes the exponential trap distribution given by,

$$P(E) = P_0 \exp\left(-\frac{E}{kT_{\mathrm{t}}}\right) \tag{4}$$

where $P(E)$ is the trap density per unit energy range at an energy E above the valence band edge. The total trap concentration of traps, N_{t}, is given as [30],

$$N_{\mathrm{t}} = P_0 kT_{\mathrm{t}} \tag{5}$$

In order to calculate the parameters P_0 and N_{t}, we need to know the dielectric constants (ε) of the investigated compounds. The values of ε were determined from capacitance measurements. Using these values of the ε and taking into account the value of the density of states N_{v} for many Pc is 10^{27} m^{-3} [31], it was found that the extracted values of N_{t} are within the range of 7.4×10^{24}–2.8×10^{25} m^{-3}. The trap concentration per unit energy range at the valence band edge varies between 2.2×10^{43} and 6.5×10^{44} J^{-1} m^{-3}. The obtained values of P_0 and N_{t} seem to be reasonable in that they are of the same order as those deduced by Abdel Malik [26] ($P_0 = 1.3 \times 10^{43}$ J^{-1} m^{-3} and $N_{\mathrm{t}} = 2.3 \times 10^{23}$ m^{-3} for CoPc films), Ahmed and Collins [32] ($P_0 = 2.79 \times 10^{43}$ J^{-1} m^{-3} and $N_{\mathrm{t}} = 2.3 \times 10^{23}$ m^{-3} for PbPc films), Gould [33] ($P_0 = 3.86 \times 10^{43}$ J^{-1} m^{-3} and $N_{\mathrm{t}} = 4 \times 10^{23}$ m^{-3} for CuPc films).

3.3. *Dielectric properties of the devices*

It was observed that the real part (ε) of the complex dielectric function decreases monotonically with increasing frequency and attains a flat value at higher frequencies for all compounds (figure 7). A reasonable explanation for the observed frequency dependence of ε can be given as follows: at low frequency, the dipoles align themselves along the field direction and fully contribute to the total polarization; as the frequency of the field is raised, the variation in the field becomes too rapid for the molecular dipoles to follow, as dipoles are unable to follow field variations at high frequencies, and are also due to electrode polarization effects, so that their contribution to the polarization becomes less, with a measurable lag, because of internal fractional forces.

It is also observed from the measurements that dielectric permittivity increases with increasing temperature. The temperature dependence of ε was weak at the high frequency region. On the other hand, it exhibited relatively strong temperature dependence at the low

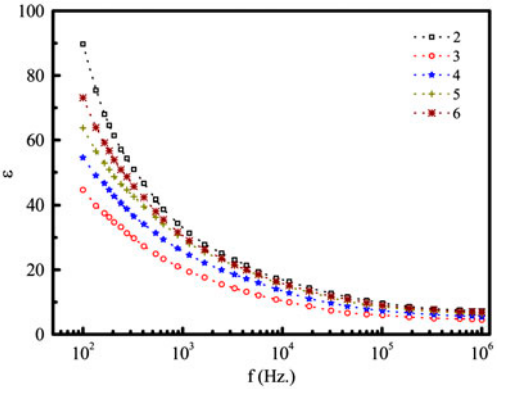

Figure 7. Frequency dependence of the real part of the dielectric function at room temperature.

frequency region. It is well known that the total polarizability of a material medium consists of various contributions such as electronic, ionic, orientation, and space charge polarization. A possible explanation for the behavior of ε with the temperature can be given as follows: at relatively low temperature, the charge carriers in most cases cannot orient themselves with respect to the direction of the applied field; therefore, they possess a weak contribution to the polarization and the dielectric constant ε. As the temperature increases, the bound charge carriers get enough excitation thermal energy to be able to obey the change in the external field more easily. This in turn enhances their contribution to the polarization leading to an increase in the dielectric constant ε of the sample [34].

3.4. *Ac conductivity study of Pc thin films*

In order to get more insight into the charge transport mechanism in MSM structures, we performed ac conductivity experiments at various temperatures. It is well established that when the localized states are randomly distributed, the ac conductivity depends on frequency as [35],

$$\sigma_{ac} = A\omega^{s} \tag{6}$$

where A is the constant, ω is the angular frequency, and the frequency exponent (s) are material dependent constants. Figure 8 shows the measured ac conductivity of the film of **5** in the frequency range 100 Hz–1 × 10^6 Hz at different temperatures. The frequency dependence of the measured ac conductivity can be represented by equation (6) for all temperatures. Different conduction mechanisms can lead to ω^s type of behavior for ac conductivity, but it is not easy to decide which mechanisms are responsible for the observed conduction. Various models such as quantum mechanical tunneling (QMT) and correlated barrier hopping (CBH) have been proposed to explain this type of frequency dependence of conductivity in disordered films. QMT model predicts a linear temperature dependence of $\sigma_{ac}(\omega,T)$ and a temperature independent s with a constant value around 0.8 which is given by,

$$s = 1 - \frac{4}{\ln(\omega\tau_0)} \tag{7}$$

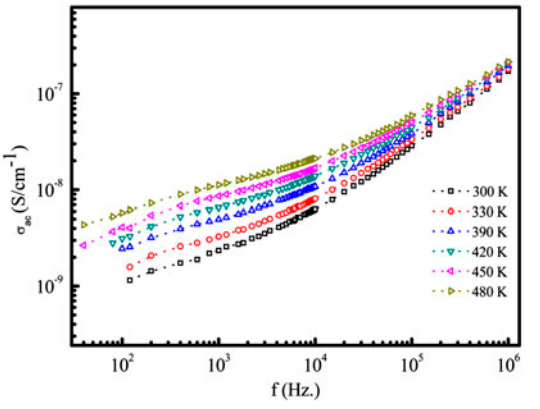

Figure 8. Variation of the ac conductivity in the film of **5** at selected temperatures.

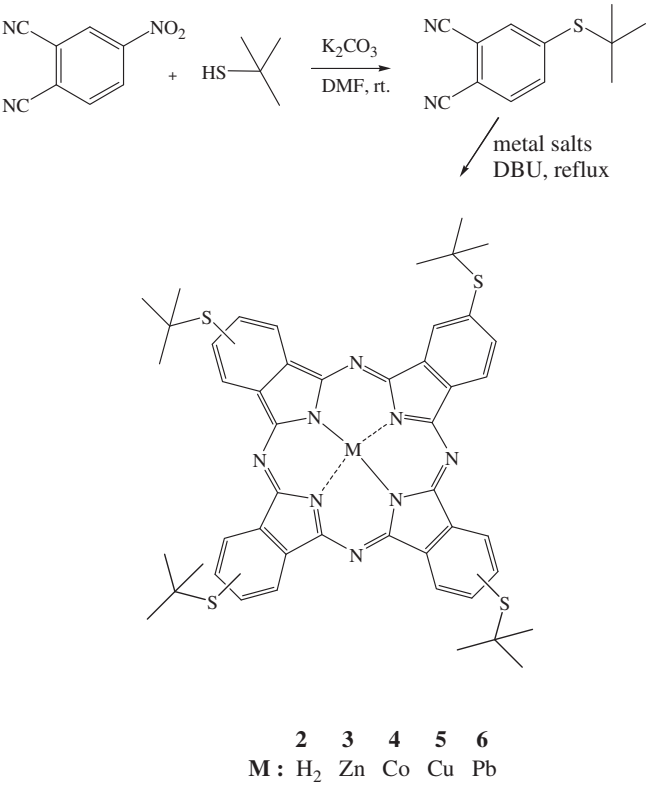

2 3 4 5 6
M : H_2 Zn Co Cu Pb

Scheme 1. Synthetic route of *tert*-butylsulfanyl-substituted phthalocyanines.

where ω is the angular frequency and τ_0 is the characteristic relaxation time of the carrier. On the other hand, according to CBH model developed by Elliott [36], charge carriers hops between sites over the potential barrier separating them rather tunneling through the barrier. The expression for conductivity in this model [36] is given by,

$$\sigma_{ac}(\omega) = \frac{\pi^2 N^2 \varepsilon}{24}\left(\frac{8q^2}{\varepsilon W_{OB}}\right)^6 \frac{\omega^s}{\tau_0^\beta} \tag{8}$$

where ε is the dielectric constant, W_{OB} is the optical band gap, τ_0 is the characteristic relaxation time, q is the electronic charge, and N is the spatial density of defect states. The frequency exponent s for this model is evaluated as,

$$s = 1 - \beta = 1 - 6k_B T/W_{OB} \tag{9}$$

where k_B is the Boltzmann's constant. To investigate the conduction mechanism involved, variation of the exponent s with temperature was examined. Values of the frequency exponent s were calculated from the straight-line fits in the logarithmic conductivity *versus* frequency plot with the aid of equation (6). It was found that the frequency exponents is definitely a function of temperature and shows a general tendency to increase with decreasing temperature. The comparison of the experimentally determined s values with the prediction of CBH model suggests that the dependence of exponent s on temperature is in agreement with the prediction of the CBH model.

4. Conclusion

New tetra *tert*-butylsulfanyl-substituted metal free and metallo (Zn, Co, Cu, and Pb) phthalocyanines have been prepared and characterized. For this purpose, the optimized synthesis of *tert*-butylsulfanylphthalonitrile compound was achieved. Bulky *tert*-butylsulfanyl substituents played an important role in high solubilities, red shifting in the Q band absorptions, and low aggregation behavior of Pc compounds. ITO/Pc/Al structures have been fabricated and current density–voltage characteristics were measured at various temperatures. It was observed that the J–V curves follow $J\alpha V^m$ power law with different slopes in the lower and higher voltage regions. The value of the mobility of charge carriers was determined from the measured characteristics. Frequency and temperature dependence of the ac conductivity have been analyzed in terms of QMT and CBH models. We have found no results supporting the QMT model. The temperature dependence of the exponent seems to support the CBH model. The dielectric investigation on these structure showed that phthalocyanine **2** is a promising dielectric with low charge mobility and relatively high dielectric constant suitable for organic-based devices such as organic field effect transistors.

Acknowledgement

The authors thank The Scientific & Technological Research Council of Turkey (TUBITAK) for financial support of this work (Project No: 111T063).

References

[1] A.M. Paoletti, G. Pennesi, G. Rossi, A. Generosi, B. Paci, V.R. Albertini. *Sensors*, **9**, 5277 (2009).
[2] M.L. Rodriguez-Mendez, J.A. de Saja. *J. Porphyrins Phthalocyanines*, **13**, 606 (2009).

[3] S. Sergeyev, E. Pouzet, O. Debever, J. Levin, J. Gierschner, J. Cornil, R.G. Aspec, Y.H. Geerts. *J. Mater. Chem.*, **17**, 1777 (2007).
[4] S. Nenon, D. Kanehira, N. Yoshimoto, F. Fages, C. Videlot-Ackermann. *Thin Solid Films*, **518**, 5593 (2010).
[5] M.G. Walter, A.B. Rudine, C.C. Wamser. *J. Porphyrins Phthalocyanines*, **14**, 759 (2010).
[6] H. Dincer, H. Mert, B.N. Sen, A. Dag, S. Bayraktar. *Dyes Pigm.*, **98**, 246 (2013).
[7] M. Abel, S. Clair, O. Ourdjini, M. Mossoyan, L. Porte. *J. Am. Chem. Soc.*, **133**, 1203 (2011).
[8] S. Samanta, A. Kumar, A. Singh, A.K. Debnath, P. Veerender, S. Basu, R. Prasad, D.K. Aswal, S.K. Gupta. *Appl. Phys. Lett.*, **100**, 162101 (2012).
[9] S. Makhseed, M. Machacek, W. Alfadly, A. Tuhl, M. Vinodh, T. Simunek, V. Novakova, P. Kubat, E. Rudolfe, P. Zimcik. *Chem. Commun.*, **49**, 11149 (2013).
[10] J. Brittona, M. Durmus, S. Khenea, V. Chaukea, T. Nyokong. *J. Porphyrins Phthalocyanines*, **17**, 691 (2013).
[11] A.B. Sorokin. *Chem. Rev.*, **113**, 8152 (2013).
[12] V.N. Nemykin, E.A. Lukyanets. *Arkivoc*, **1**, 136 (2010).
[13] K.M. Kadish, K.M. Smith, R. Guilard (Eds). *Porphyrin and Phthalocyanine Handbook*, Vols. 11–20, Academic Press, Boston, MA (2003).
[14] D.A. Fernández, J. Awruch, E. Lelia, L.E. Dicelio. *Photochem. Photobiol.*, **63**, 84 (1996).
[15] E.M. Maya, P.A. Vaazquez, T. Torres. *Chem. Eur. J.*, **5**, 2004 (1999).
[16] L.A. Valkova, L.S. Shabyshev, N.Y. Borovkov, L.A. Feigin, F. Rustichelli. *J. Inclusion Phenom. Macrocyclic Chem.*, **35**, 243 (1999).
[17] B.N. Sen, H. Mert, H. Dincer, A. Koca. *Dyes Pigm.*, **100**, 1 (2014).
[18] E.H. Morkved, F.M. Pedersen, N.K. Afseth, H. Kjosen. *Dyes Pigm.*, **77**, 145 (2007).
[19] M. Kostkaa, P. Zimcik. *J. Photochem. Photobiol., A*, **178**, 16 (2006).
[20] K.I. Ozoemena, T. Nyokong. *Inorg. Chem. Commun.*, **6**, 1192 (2003).
[21] H.A. Dincer, A. Gül, M.B. Kocak. *Dyes Pigm.*, **74**, 545 (2007).
[22] O.V. Dolotova, N.I. Bundına, V.M. Derkacheva, V.M. Negrimovskii, V.V. Minin, G.M. Larin, O.L. Kaliya, E.A. Lukyanets. *Zh. Obshch. Khimi.*, **62**, 2064 (1992).
[23] D. Wöhrle, L. Kreienhoop, G. Schnurpfeil, J. Elbe, B. Tennigkeit, S. Hiller, D. Schlettwein. *J. Mater. Chem.*, **5**, 1819 (1995).
[24] Z. Odabaş, A. Altindal, A.R. Ozkaya, B. Salih, Ö. Bekaroğlu. *Sens. Actuators B*, **145**, 355 (2010).
[25] H.M. Zeyada, M.M. El-Nahass. *Appl. Surf. Sci.*, **254**, 1852 (2008).
[26] T.G. AbdelMalik, R.M. Abdel-Latif. *Thin Solid Films*, **305**, 336 (1997).
[27] W. Gao, A. Kahn. *Org. Electron.*, **3**, 53 (2002).
[28] S.I. Shihub, R.D. Gould. *Thin Solid Films*, **290–291**, 390 (1996).
[29] T.D. Anthopoulos, T.S. Shafia. *Phys. Status Solidi A*, **186**, 89 (2001).
[30] R.D. Gould, M.S. Rahman. *J. Phys. D*, **14**, 79 (1981).
[31] A. Sussman. *J. Appl. Phys.*, **38**, 2738 (1967).
[32] A. Ahmed, R.A. Collins. *Phys. Status Solidi A*, **123**, 201 (1991).
[33] R.D. Gould. *J. Phys. D: Appl. Phys.*, **9**, 1785 (1986).
[34] M.R. Anantharaman, S. Sindhu, S. Jagatheesan, K.A. Molini, P. Kurian. *J. Phys. D*, **32**, 1801 (1999).
[35] M. Pollak, T.H. Geballe. *Phys. Rev.*, **122**, 1742 (1961).
[36] S.R. Elliott. *Adv. Phys.*, **36**, 135 (1987).